British Geological Survey
NATURAL ENVIRONMENT RESEARCH COUNCIL

LC1DINV: Laterally-Constrained 1-D Inversion for Processing Airborne EM Data

NATIONAL GEOSCIENCE FRAMEWORK PROGRAMME
Internal Report IR/05/118

BRITISH GEOLOGICAL SURVEY

NATIONAL GEOSCIENCE FRAMEWORK PROGRAMME

INTERNAL REPORT IR/05/118

LC1DINV: Laterally-Constrained 1-D Inversion for Processing Airborne EM Data

E Tartaras

Contributor/editor

D Beamish

Keywords

airborne; EM; inversion.

Front cover

EM coils on airborne system.

Bibliographical reference

TARTARAS, E. 2005. LC1DINV: Laterally-Constrained 1-D Inversion for Processing Airborne EM Data. *British Geological Survey Internal Report*, IR/05/118. 15pp.

Keyworth, Nottingham British Geological Survey 2005

BRITISH GEOLOGICAL SURVEY

The full range of Survey publications is available from the BGS Sales Desks at Nottingham, Edinburgh and London; see contact details below or shop online at www.geologyshop.com

The London Information Office also maintains a reference collection of BGS publications including maps for consultation.

The Survey publishes an annual catalogue of its maps and other publications; this catalogue is available from any of the BGS Sales Desks.

The British Geological Survey carries out the geological survey of Great Britain and Northern Ireland (the latter as an agency service for the government of Northern Ireland), and of the surrounding continental shelf, as well as its basic research projects. It also undertakes programmes of British technical aid in geology in developing countries as arranged by the Department for International Development and other agencies.

The British Geological Survey is a component body of the Natural Environment Research Council.

British Geological Survey offices

Keyworth, Nottingham NG12 5GG

☎ 0115-936 3241 Fax 0115-936 3488
e-mail: sales@bgs.ac.uk
www.bgs.ac.uk
Shop online at: www.geologyshop.com

Murchison House, West Mains Road, Edinburgh EH9 3LA

☎ 0131-667 1000 Fax 0131-668 2683
e-mail: scotsales@bgs.ac.uk

London Information Office at the Natural History Museum (Earth Galleries), Exhibition Road, South Kensington, London SW7 2DE

☎ 020-7589 4090 Fax 020-7584 8270
☎ 020-7942 5344/45 email: bgslondon@bgs.ac.uk

Forde House, Park Five Business Centre, Harrier Way, Sowton, Exeter, Devon EX2 7HU

☎ 01392-445271 Fax 01392-445371

Geological Survey of Northern Ireland, Colby House, Stranmillis Court, Belfast, BT9 5BF

☎ 028-9038 8462 Fax 028-9038 8461

Maclean Building, Crowmarsh Gifford, Wallingford, Oxfordshire OX10 8BB

☎ 01491-838800 Fax 01491-692345

Sophia House, 28 Cathedral Road, Cardiff, CF11 9LJ

☎ 029–2066 0147 Fax 029–2066 0159

Parent Body

Natural Environment Research Council, Polaris House, North Star Avenue, Swindon, Wiltshire SN2 1EU

☎ 01793-411500 Fax 01793-411501
www.nerc.ac.uk

Foreword

This report describes the one-dimensional laterally constrained inversion algorithm "LC1DINV" that we have developed for the interpretation of airborne electromagnetic data.

The first part of the report introduces the problem and addresses the need for this work. The second part describes the mathematical development of the algorithm and its main characteristics. Finally, the third part shows examples of the application of this algorithm to synthetic data sets.

Contents

Foreword ..... **i**

Contents ..... **i**

Summary ..... **ii**

1 Introduction **3**

2 Frequency-domain AEM inversion methods **3**

3 LC1DINV algorithm development and description **3**

3.1 Lateral constraints implementation 4

3.2 Regularised Conjugate Gradient minimisation routine 5

4 Application of LC1DINV on synthetic AEM data sets **8**

4.1 1-D models 8

4.2 3-D models 11

5 Conclusions **14**

References **14**

FIGURES

Figure 1. Simulated model of a conductive half-space below a resistive top layer. 8

Figure 2. LC1DINV inversion result without lateral constraints and with no added noise. 9

Figure 3. LC1DINV inversion result without lateral constraints and with 5% added noise. ... 10

Figure 4. LC1DINV inversion result with lateral constraints and with 5% added noise. 10

Figure 5. Simulated 3-D model of a conductive surface target in two-layer earth..... 11

Figure 6. LC1DINV inversion results for four flight lines, using a two-layer model. 12

Figure 7. LC1DINV inversion results for four flight lines, using a three-layer model. 13

Summary

BGS has recently developed jointly with GTK (Geological Survey of Finland) an advanced airborne geoscience capability and has commenced extended airborne surveying of Northern Ireland with other areas soon to follow. Large multi-frequency electromagnetic data sets comprise an important part of these surveys. In order to aid the interpretation of these data sets, we have developed “LC1DINV”, a laterally constrained one-dimensional inversion algorithm.

LC1DINV inverts for the resistivities and thicknesses of a few (two or three) horizontal layers using a regularised conjugate gradient optimisation routine. The inverse problem is stabilised through the use of lateral constraints that ensure that model parameters change smoothly in the horizontal direction while preserving our ability to distinguish layer boundaries. Tests on synthetic models confirm the stability and efficiency of the method.

1 Introduction

BGS has developed jointly with GTK (Geological Survey of Finland) an advanced airborne geoscience capability and has commenced extended airborne surveys in Northern Ireland and elsewhere. An important part of these surveys is the acquisition of large multi-frequency electromagnetic (EM) data sets in order to characterise the conductivity distribution of the subsurface. We therefore need a fast and reliable way to invert large airborne electromagnetic (AEM) data sets. This report describes the laterally constrained one-dimensional (1-D) inversion algorithm "LC1DINV" that we have developed for this purpose.

2 Frequency-domain AEM inversion methods

AEM surveys produce large data sets that require fast and stable inversion tools. Industry standard practice for interpretation of frequency-domain AEM data is to use half-space inversions, i.e. apparent resistivity transformations, that invert for the resistivity of a half-space and its depth below the receiver (Fraser, 1978; Fraser 1986, Huang and Fraser, 1996). These transformations are not only very fast but they are also very stable because one can always find a half-space resistivity that will fit the data. Moreover, errors in flight altitude do not affect the apparent resistivity estimation but are propagated into the apparent depth estimation. They can therefore produce a good representation of horizontal resistivity variations. However, they don't allow detection of resistivity variations with depth and suffer in areas where the resistivity model departs significantly from that of a half-space.

In order to distinguish vertical resistivity variations and obtain a formal measure of model validity one can use a multi-layer 1-D inversion (Beard, 2000; Beard and Nyquist, 1998; Constable et al., 1987; Ellis, 1998; Fitterman and Deszcz-Pan, 1998; Paterson and Redford, 1986; Sengpiel and Siemon, 1998, 2000). These inversions are non-unique because they solve a heavily underdetermined problem. They therefore utilise additional constraints in order to stabilise the problem, such as the smoothness constraint that requires that vertical resistivity variations in the model be smooth. Inversions of this type manage to successfully fit the data but produce very smooth sections where formation boundaries are smeared and are difficult to distinguish.

In areas where the geology departs from the 1-D assumption (isolated anomalies, dipping targets, etc.) three-dimensional (3-D) inversion may be necessary. Full non-linear 3-D EM inversion (e.g., Sasaki, 2001; Sasaki and Nakazato, 2003) is, however, very time-consuming and unsuitable for airborne surveys which produce very large data sets from multiple transmitter positions. Attempts to develop fast and practical 3-D inversion schemes based on approximations have recently been made and some of these algorithms have been applied to AEM data (Zhang, 2003; Zhdanov and Tartaras, 2002), but these methods can be still applied only to limited areas of particular interest.

3 LC1DINV algorithm development and description

Given a starting model, m, that describes the (electrical) parameters of the subsurface, the main objective of an inversion algorithm is to gradually modify this model until the *predicted* data, d_p, match the *observed* data, d, to a satisfactory degree. The predicted data are computed using a numerical modelling code that incorporates the appropriate physics of the problem. The difference between predicted and observed data is the data *misfit*. The starting model is gradually modified according to an optimization routine so as to reduce the data misfit.

We have constructed a 1-D inversion scheme, which means that the electrical parameters of the subsurface vary only in one direction, namely with depth. Thus our model consists of a series of horizontal layers and the model parameters comprise the resistivities and thicknesses of these layers. The number of layers is unlimited but when a two-frequency airborne system is used we only use two or three-layer models in the inversion, because we are unable to resolve more layers. We use the 1-D modelling code "BLOOPS" (Sinha, 1977) to compute the predicted data.

As stated, the goal of an inversion algorithm is to gradually reduce the misfit between predicted and observed data. The distance between the two data sets can be defined in a few different ways. We have used the L_2 norm, $\|...\|$, of the data differences, which is calculated as the square root of the sum of the squares of the differences between individual data points: $\|d - d_p\| = \sqrt{\sum_i \left(d^i - d_p^i\right)^2}$. Ideally, we would like to match the observed data exactly. In practice, however, noise, incomplete data coverage and imperfect model parameterization limit our ability to do so. Therefore, we try instead to match the observed data to a desired level of accuracy, ε. As a result of the above limitations, the inverse problem is *ill posed*, i.e., unstable and non-unique. In order to find a stable solution we *regularise* the problem by imposing additional conditions that our model needs to satisfy (Tikhonov and Arsenin, 1977). There are several possible choices for these additional conditions with a widely used one being the smoothness constraint (Loke and Barker, 1996; Oldenburg and Li, 1994). The problem with this type of constraint is that it produces smooth models where it is difficult to distinguish boundaries between formations. We opt instead for a *laterally constrained* inversion (Auken et al., 2002; Auken and Christiansen, 2004; Christiansen and Auken, 2004; Smith et al., 1999; Wisen et al., 2005). In this type of inversion we invert simultaneously for several observation points and we require that lateral changes in the model parameters from one observation point to the next are small. Thus, we retain the ability to distinguish different layers while we avoid the problem common to many 1-D inversion schemes of "noisy"-looking resulting models. Moreover, we may, if we have such information, require our model to be close to an *apriori* model, m_{apr}.

Mathematically the above requirements mean that instead of just trying to minimise the data misfit, we try to minimise the parametric functional $P(m) = \phi(m) + \alpha Sm(m) + \beta Sr(m)$, where α and β are regularisation parameters, ϕ is the misfit functional and Sm and Sr are stabilising functionals:

$$\phi(m) = W_d \left\| d_p - d \right\|^2,$$

$$Sm(m) = W_m \left\| m - m_{apr} \right\|,$$

$$Sr(m) = W_m \left\| Rm \right\|.$$

W_d and W_m are data and model weighting matrices respectively, and R is the "roughening" matrix that implements the lateral constraints. The next two subsections describe in detail the implementation of the lateral constraints and the optimisation routine used to minimise the parametric functional.

3.1 LATERAL CONSTRAINTS IMPLEMENTATION

The lateral constraints are implemented through the use of a *roughening* matrix, R, that is applied to the vector of model parameters, m. The roughening matrix contains 1 and –1's for the constrained parameters and 0 at all other places. For example the first row of the roughening matrix has 1 in the first column that corresponds to the first parameter, i.e., the resistivity of the first layer, for observation point #1 and –1 at the column that corresponds to the same parameter but for observation point #2. The same is true for the columns that correspond to the other

parameters (thickness of the first layer, resistivity of the second layer and so forth). The second row has 1 and –1 for the same parameters but for observation points #2 and #3. Thus matrix R has a banded form:

$$R = \begin{bmatrix} 1 & 0 & \cdots & 0 & -1 & 0 & \cdots & 0 & 0 & 0 \\ 0 & 1 & 0 & \cdots & 0 & -1 & 0 & \cdots & 0 & 0 \\ \vdots & & & & & \vdots & & & & \vdots \\ 0 & 0 & 0 & \cdots & 0 & 1 & 0 & \cdots & 0 & -1 \end{bmatrix}$$

The effect of the roughening matrix is that it penalises large differences between parameters of adjacent points.

3.2 REGULARISED CONJUGATE GRADIENT MINIMISATION ROUTINE

In order to find the minimum of the parametric functional we use the conjugate gradient (CG) method (Hestenes and Stiefel, 1952). This is a local minimisation method that belongs to the large family of gradient-type methods. The main idea of this method is based on the (simpler) steepest descent method which always finds the direction that locally minimises the functional in question. However, that method converges slowly because the search directions are not sufficiently different from each other. Therefore, in the CG method, every new search direction is taken to be a linear combination of the current steepest descent direction and the previous search directions in order to obtain a search direction that is *conjugate* to the previous ones. The basic CG algorithm can be described as follows (Golub and Van Loan, 1996):

$m = initial\ guess; \quad n = 0; \quad r = Am - d; \quad \phi = \|r\|^2$
$while \left(\sqrt{\phi_n} > \varepsilon \|d\|\right) \wedge \left(n < n_{\max}\right)$
  $n = n + 1$
  $if\ n = 1$
    $p = r$
  $else$
    $\beta_n = \phi_{n-1} / \phi_{n-2}$
    $p = r + \beta_n p$
  end
  $w = Ap; \quad \alpha_n = \phi_{n-1} / p^T w$
  $m = m + \alpha_n p; \quad r = r - \alpha_n w$
  $\phi_n = \|r\|^2$
end

The CG method as described above was originally developed for the solution of linear systems. Here we use this method for the solution of a non-linear inverse problem. In this case at each iteration we need to compute the Jacobian (or sensitivity) matrix,

$$F = \frac{\partial A(m)}{\partial m} = \frac{A(m + \delta m) - A(m)}{\delta m},$$

where A is the forward modelling operator. The elements of the Jacobian matrix are calculated as the change observed in the data point d_i for a small change in the model parameter m_j:

$$F_{ij} = \frac{\partial d_i}{\partial m_j}.$$

Then, the CG algorithm can be described as follows (Zhdanov, 2002):

$$
\begin{aligned}
&m = initial\ guess; \quad n = 0; \quad g_0 = 0; \quad \phi = \|r\|^2 \\
&while\ \left(\sqrt{\phi} > \varepsilon\|d\|\right) \wedge \left(n < n_{\max}\right) \\
&\quad n = n + 1 \\
&\quad r = A(m) - d \\
&\quad \phi = \|r\|^2 \\
&\quad F = \partial A(m)/\partial m \\
&\quad l_n = F^T r \\
&\quad \beta_n = \|l_n\|^2 / \|l_{n-1}\|^2 \\
&\quad g_n = l_n + \beta_n g_{n-1} \\
&\quad k_n = l_n^{\ T} g_n / \|F g_n\|^2 \\
&\quad m = m - k_n g_n \\
&end
\end{aligned}
$$

where l_n is the steepest descent direction and g_n is the conjugate direction at the n^{th} iteration.

However, the non-linear problem we are trying to solve is ill posed and we have regularised it by adding additional constraints, namely the lateral constraints and the apriori information. We thus want to minimise the parametric functional, i.e. we require that $P(m) = \phi(m) + \alpha Sm(m) + \beta Sr(m) \equiv \min$. To solve this problem we take the first derivative of the parametric functional with respect to the model, *m*, and set it to zero. Using differential calculus we derive the final form of the regularised CG method:

$$
\begin{aligned}
&m = initial\ guess; \quad n = 0; \quad g_0 = 0; \quad \phi = \|r\|^2 \\
&while\ \left(\sqrt{\phi} > \varepsilon\|d\|\right) \wedge \left(n < n_{\max}\right) \\
&\quad n = n + 1 \\
&\quad r = A(m) - d \\
&\quad \phi = \|r\|^2 \\
&\quad F = \partial A(m)/\partial m \\
&\quad l_n = F^T W_d^{\ 2} r + \alpha W_m^{\ 2}\left(m - m_{apr}\right) + \beta R^T W_R^{\ 2} R m \\
&\quad \beta_n = \|l_n\|^2 / \|l_{n-1}\|^2 \\
&\quad g_n = l_n + \beta_n g_{n-1} \\
&\quad k_n = \frac{l_n^{\ T} g_n}{\|W_d F g_n\|^2 + \alpha\|W_m g_n\|^2 + \beta\|W_R R g_n\|^2} \\
&\quad m = m - k_n g_n \\
&end
\end{aligned}
$$

3.2.1 Discretised (matrix) form

The vectors and matrices of the inverse problem we are solving have the following dimensions:

d = Nd-by-1 (data vector)

m = Nm-by-1 (model parameter vector)

W_d = Nd-by-Nd (data weighting matrix)

W_m = Nm-by-Nm (model weighting matrix)

W_R = Nc-by-Nc (lateral-constraint weighting matrix)

F = Nd-by-Nm (Jacobian matrix)

R = Nc-by-Nm (roughening matrix),

where Nd=2*Nf*Nobs is the total number of measurements (data), Nf is the number of frequencies in use, Nobs is the number of observation points, Nm=Npar*Nobs is the total number of model parameters, Npar=2*Nl-1 is the number of model parameters per observation point, Nl is the number of layers comprising the model, Nc = Npar*(Σ(1:Nlatc)+Nlatc*(Nobs-Nlatc-1)) is the total number of lateral constraints, Nlatc is the number of lateral constraints either side of each observation point, and 1:Nlatc is the vector with elements the sequence of numbers from 1 to Nlatc.

Thus, the CG routine in discretised (matrix) form looks as follows:

$m = initial\ guess; \quad n = 0; \quad g_0 = 0; \quad \phi = r^T r$

$while\ \left(\sqrt{\phi} > \varepsilon \|d\|\right) \wedge \left(n < n_{\max}\right)$

$n = n + 1$

$r = A(m) - d$

$\phi = r^T r$

$for\ i = 1 : Nd$

$for\ j = 1 : Nm$

$$F_{ij} = \frac{\partial d_i}{\partial m_j}$$

end

end

$$l_n = F^T W_d{}^2 r + \alpha W_m{}^2 \left(m - m_{apr}\right) + \beta R^T W_R{}^2 R m$$

$$\beta_n = \frac{l_n{}^T l_n}{l_{n-1}{}^T l_{n-1}}$$

$$g_n = l_n + \beta_n g_{n-1}$$

$$k_n = \frac{l_n{}^T g_n}{g_n{}^T F^T W_d{}^2 F g_n + \alpha g_n{}^T W_m{}^2 g_n + \beta g_n{}^T R^T W_R{}^2 R g_n}$$

$$m = m - k_n g_n$$

end

4 Application of LC1DINV on synthetic AEM data sets

In order to test and demonstrate the effectiveness of our algorithm we inverted synthetic data sets computed for 1-D and 3-D models. We used the numerical modelling package "EMIGMA", distributed by PetRos EiKon Inc., for these calculations. EMIGMA computes the 3-D responses using algorithms based on the localized non-linear (LN) approximation of the integral equation for the electric field (Habashy et al., 1993; Murray, 1997; Murray et al., 1999). The data sets comprise four components: real (in-phase) and imaginary (quadrature) for each of two frequencies. The two frequencies used here are 3 and 14 kHz, being those of the current AEM system.

4.1 1-D MODELS

We first need to test whether LC1DINV can successfully recover a 1-D conductivity distribution and how the use of lateral constraints affects/improves the inversion results. Therefore, we simulated an AEM survey over a simple two-layer earth and inverted the synthetic data with and without the use of lateral constraints. The simulated airborne system is the one used by BGS: two pairs of vertical coplanar coils operating at 3 and 14 kHz with a transmitter-receiver separation of 21.36m. Measurements were simulated every 10 m along the flight path.

Figure 1 shows the simulated model which comprises a 40m-thick surface layer with conductivity 10 mS/m and a lower half-space with conductivity 50 mS/m. Figure 2 shows the result of the inversion without the use of lateral constraints. In this case no noise was added to the data and it is obvious that the recovered conductivity distribution matches closely the true one. Actually the only difference between the recovered and true conductivity distributions is that the bottom layer is shown to be a little more conductive and a little deeper than that of the synthetic model. This difference is simply due to the parameter equivalence inherent in the EM inverse problem.

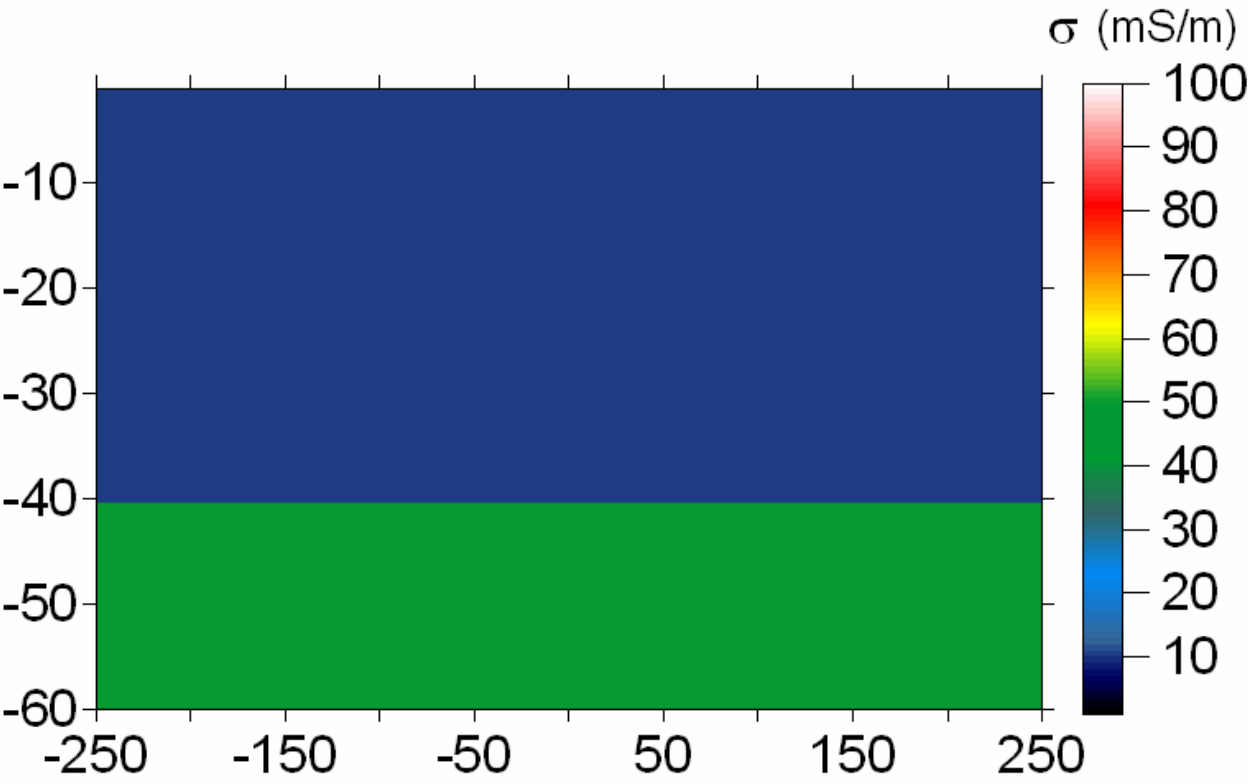

Figure 1. Simulated model of a conductive half-space below a resistive top layer.

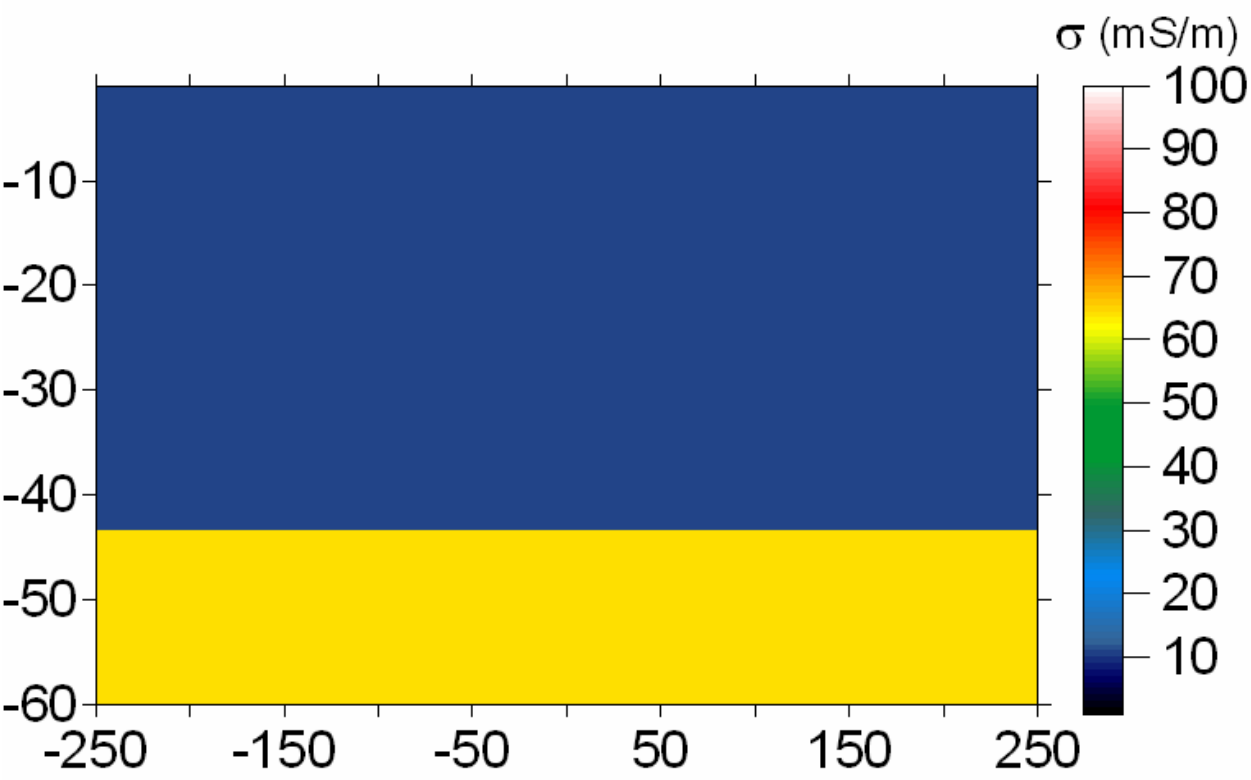

Figure 2. LC1DINV inversion result without lateral constraints and with no added noise.

However, when we add 5% noise and re-invert the data, the resulting conductivity cross-section (shown in Figure 3) is very “noisy”. This is actually a typical characteristic of 1-D inversions due to noise and other problems in survey data (e.g., small errors in the altitude estimation). The use of lateral constraints significantly helps to alleviate this problem, as is evident in the inversion result of Figure 4. Here we inverted the same noisy data but this time we applied the lateral constraints in the LC1DINV algorithm, using Nlatc=1, i.e. one lateral constraint on either side of each observation point. The “noisy” look has disappeared, the conductivity cross-section shows a remarkable continuity in the horizontal direction and it still closely matches the true conductivity distribution.

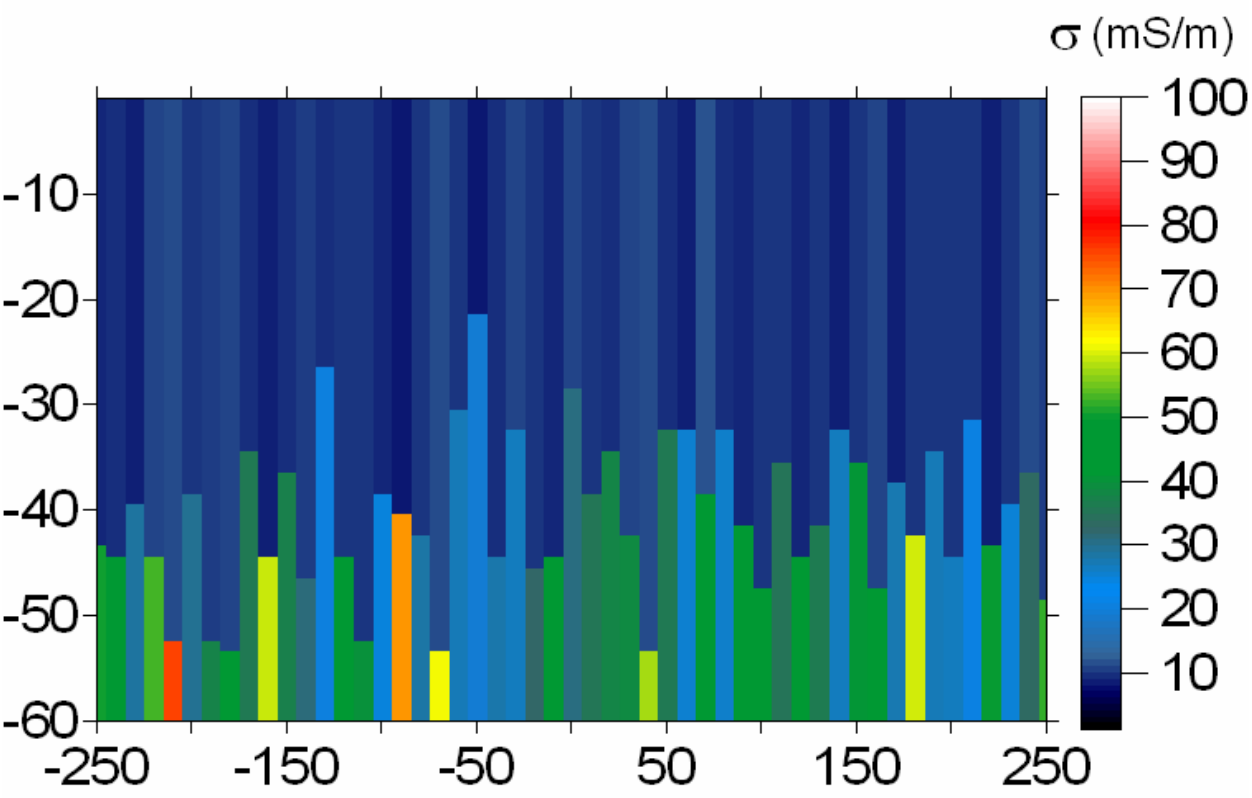

Figure 3. LC1DINV inversion result without lateral constraints and with 5% added noise.

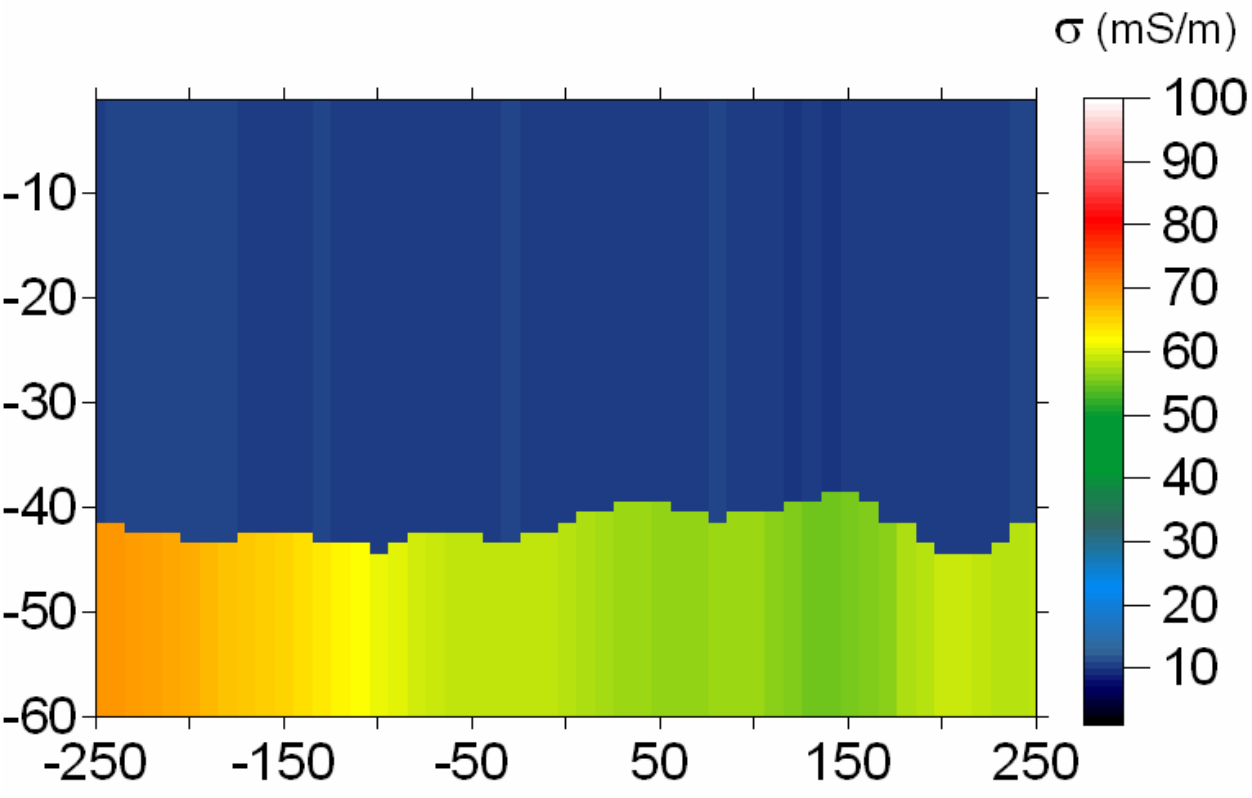

Figure 4. LC1DINV inversion result with lateral constraints and with 5% added noise.

4.2 3-D MODELS

In reality, however, the subsurface conductivity distribution rarely conforms to a 1-D model. Often there exist 3-D anomalies that can either be targets or sources of noise, depending on the survey objectives. Here we have simulated a 3-D model based on the 1-D model of the previous section and the addition of a conductive surface body. The conductivity of the 3D body is 50 mS/m, its thickness is 10 m and its horizontal extent is 100 m in both directions. We have simulated several flight lines across the body with a measurement interval of 10 m along the flight path and a flight line separation of 50 m. Figure 5 shows a cross-section across the centre of the simulated model. The model outside the area of the conductive surface body is the 1-D model of Figure 1. 5% random noise was added to all the data before inversion and the lateral constraints (with Nlatc=1) were applied to regularise the problem. Figure 6 shows the inversion results, using a two-layer model, for four flight lines passing over the centre of, over the edge of, 100 metres away and 200 metres away from the 3-D surface target, respectively. We can see that outside the anomaly, the inversion algorithm quite successfully recovers the correct conductivity distribution. Over the conductive body, however, the two-layer model is unable to correctly represent the conductivity distribution. A slight increase in conductivity is observed at the centre of the profile without however reaching the true value of 50 mS/m.

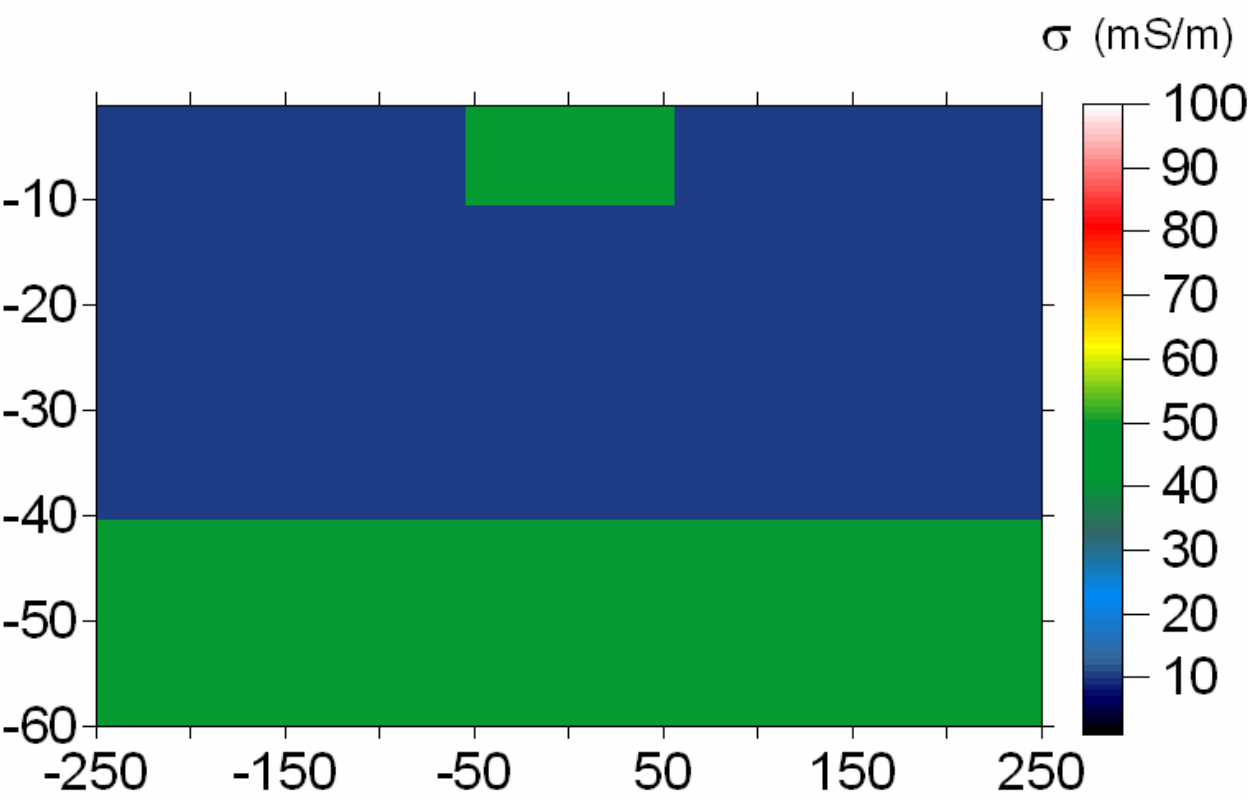

Figure 5. Simulated 3-D model of a conductive surface target in two-layer earth.

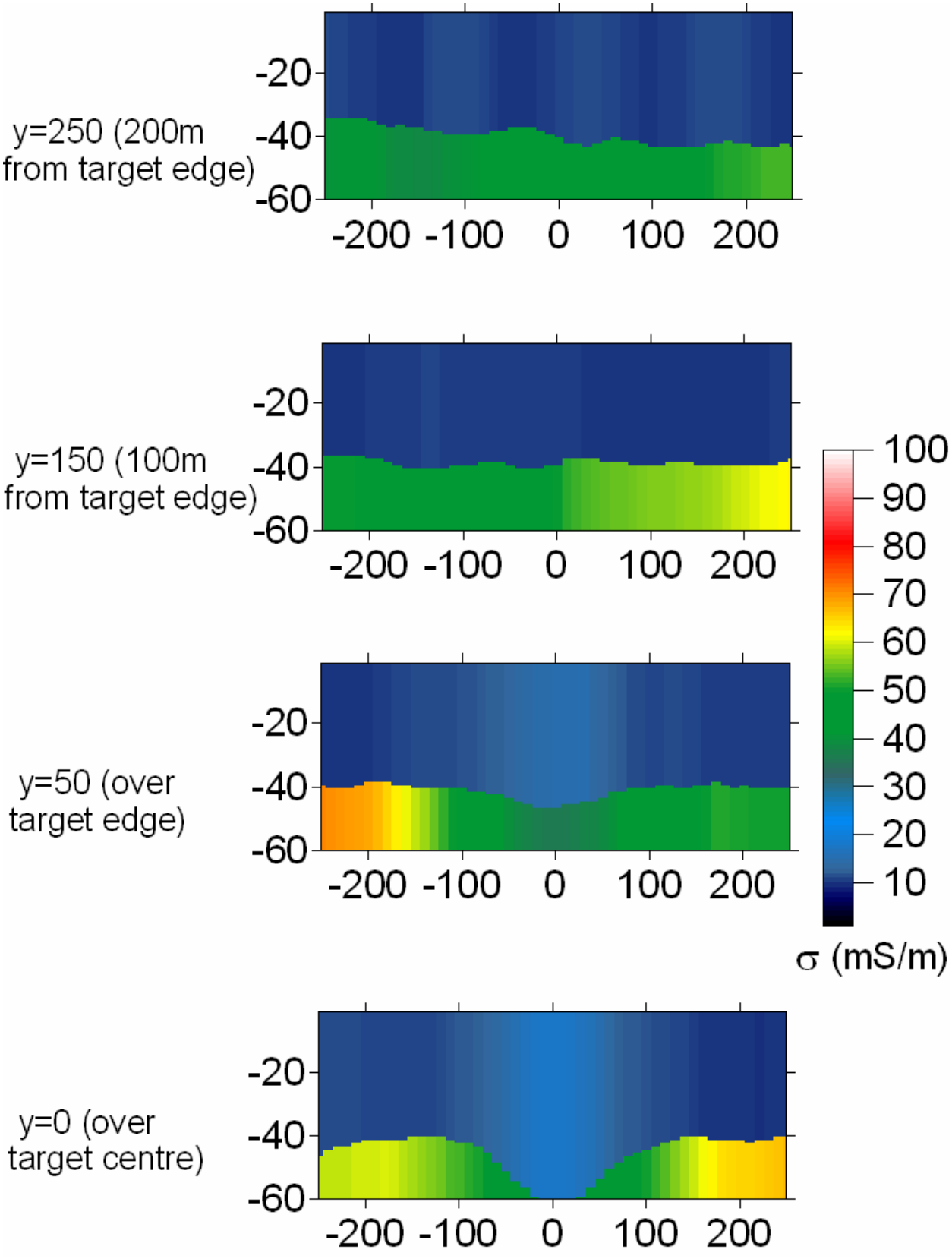

Figure 6. LC1DINV inversion results for four flight lines, using a two-layer model.

Figure 7 shows the inversion results for the same flight lines but this time using a three-layer model. We can see that this time the conductive body is identified more clearly, although its conductivity is still underestimated. Outside the extent of the anomaly, the use of a three-layer model results in a slight overestimation of the conductivity between depths of 20 and 40 metres. Actually, a three-layer model corresponds to five model parameters and since our data only have

four components, this is an underdetermined problem. It is thus evident that a two-layer model is satisfactory and even preferable in most cases and a three-layer model is useful for inverting data over certain areas where the presence of a surface anomaly or a more complicated geology has been identified.

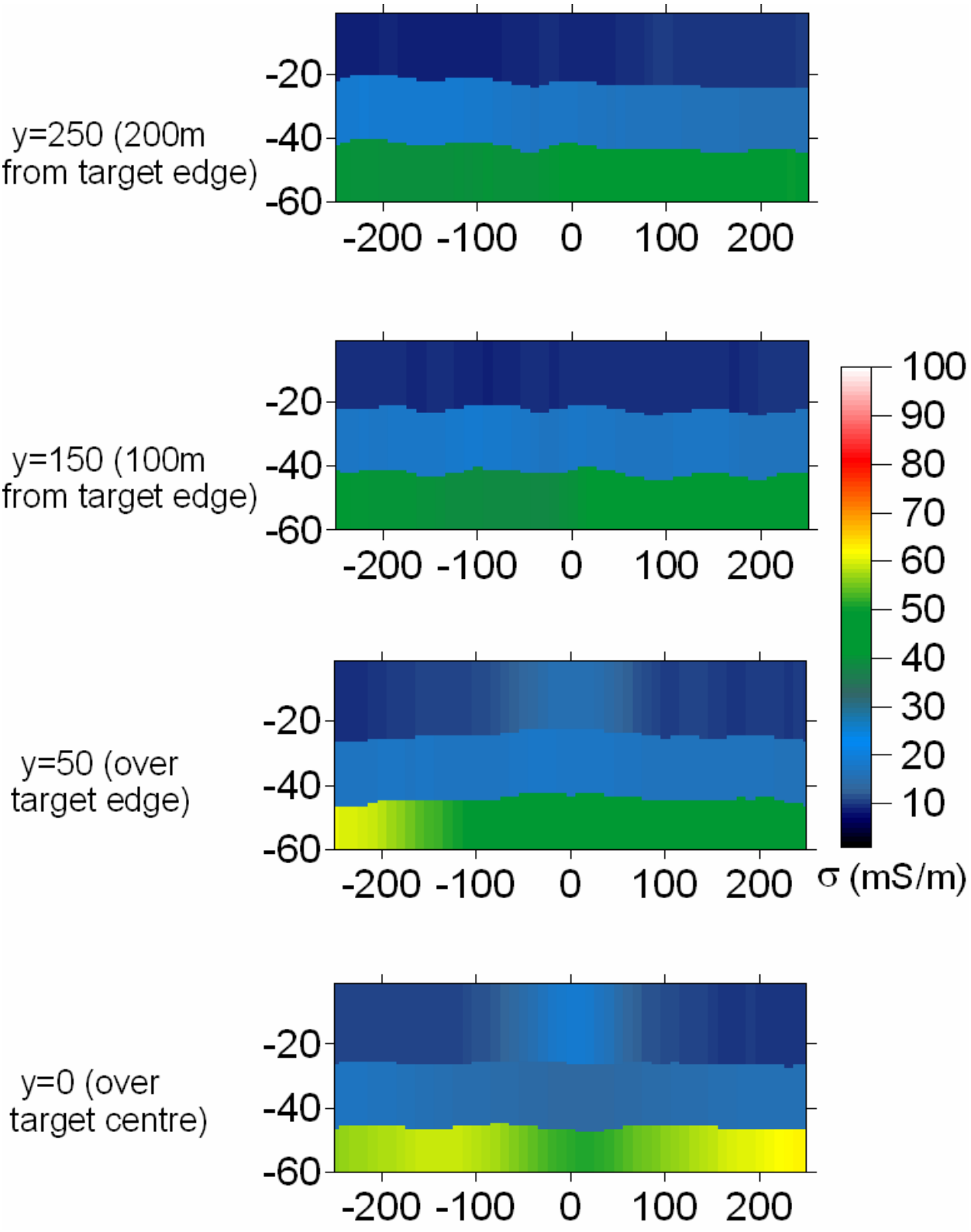

Figure 7. LC1DINV inversion results for four flight lines, using a three-layer model.

5 Conclusions

The application of LC1DINV to synthetic AEM data sets has shown that it is a stable algorithm that successfully recovers the subsurface distribution of conductivity and produces cross-sections that do not suffer from the "noisy" look common to multi-layer 1-D inversions. Moreover, it produces laterally smooth sections, while preserving the ability to distinguish distinct horizontal layers and formation boundaries. It is therefore a very useful tool for a more advanced interpretation of large airborne EM data sets, beyond the common deliverable of half-space apparent resistivity.

References

AUKEN, E., CHRISTIANSEN, A V., JACOBSEN, B H., FOGED, N., and SORENSEN, K I. 2002. Piecewise 1D laterally constrained inversion of resistivity data. *Geophysical Prospecting*, Vol. 53, no. 4, 497–506.

AUKEN, E., and CHRISTIANSEN, A V. 2004. Layered and laterally constrained 2D inversion of resistivity data. *Geophysics*, Vol. 69, no. 3, 752–761.

BEARD, L P. 2000. Comparison of methods for estimating earth resistivity from airborne electromagnetic measurements. *Journal of Applied Geophysics*, Vol. 45, 239–259.

BEARD, L P., and NYQUIST, J E. 1998. Simultaneous inversion of airborne electromagnetic data for resistivity and magnetic permeability. *Geophysics*, Vol. 63, 1556–1564.

CHRISTIANSEN, A V. and AUKEN, E. 2004. Optimising a layered and laterally constrained 2D inversion of resistivity data using Broyden's update and 1D derivatives. *Journal of Applied Geophysics*, Vol. 56, no. 4, 247–261.

CONSTABLE, S C., PARKER, R L., and CONSTABLE, C G. 1987. Occam's inversion: a practical algorithm for generating smooth models from electromagnetic sounding data. *Geophysics*, Vol. 67 289–300.

ELLIS, R G. 1998. Inversion of airborne electromagnetic data. *Exploration Geophysics*, Vol. 29, 121–127.

FITTERMAN, D V., and DESZCZ-PAN, M. 1998. Helicopter EM mapping of saltwater intrusion in Everglades National Park. *Exploration Geophysics*, Vol. 29, 240–243.

FRASER, D C. 1978. Resistivity mapping with an airborne multicoil electromagnetic system. *Geophysics*, Vol. 43, 144–172.

FRASER, D C. 1986. Dighem resistivity techniques in airborne electromagnetic mapping. 49–54 in *Airborne resistivity mapping*. PALACKY G J. (editor). (Geological Survey of Canada.)

GOLUB, G H., and VAN LOAN, C F. 1996. *Matrix Computations, 3rd ed.* (Baltimore: The John Hopkins University Press.)

HABASHY, T M., GROOM, R W., and SPIES, B R. 1993. Beyond the Born and Rytov approximations: a nonlinear approach to electromagnetic scattering. *Journal of Geophysical Research*, Vol. 98, no. B2, 1759–1775.

HESTENES, M R., and STIEFEL, E. 1952. Methods of conjugate gradients for solving linear systems. *J. Res. Natl. Bur. Stand.*, Vol. 49, 409–436.

HUANG, H., and FRASER, D C. 1996. The differential parameter method for multi-frequency airborne resistivity mapping. *Geophysics*, Vol. 55, 1327–1337.

HUANG, H., and FRASER, D C. 1996. The differential parameter method for multi-frequency airborne resistivity mapping. *Geophysics*, Vol. 55, 1327–1337.

LOKE, M H., and BARKER, R D. 1996. Rapid least-squares inversion of apparent resistivity pseudosections by quasi-Newton method. *Geophysical Prospecting*, Vol. 44, 131–152.

MURRAY, I R. 1997. On extending the localized non-linear approximator to inductive modes. *Extended Abstracts*, F004, 59th EAGE Conference, Geneva, Switzerland.

MURRAY, I R., ALVAREZ, C., and GROOM, R W. 1999. Modelling of complex electromagnetic targets using advanced non-linear approximator techniques. *Extended Abstracts*, 69th SEG Conference, Houston, Texas, USA.

OLDENBURG, D W., and LI, Y. 1994. Inversion of induced polarization data. *Geophysics*, Vol. 59, 1327–1341.

PATERSON, N R., and REDFORD, S W. 1986. Inversion of airborne electromagnetic data for overburden mapping and groundwater exploration. 39–48 in *Airborne resistivity mapping*. PALACKY G J. (editor). (Geological Survey of Canada.)

SASAKI, Y. 2001. Full 3-D inversion of electromagnetic data on PC. *Journal of Applied Geophysics*, Vol. 46, 45–54.

SASAKI, Y., and NAKAZATO, H. 2003. Topographic effects in frequency-domain helicopter-borne electromagnetics. *Exploration Geophysics*, Vol. 34, 24–28.

SENGPIEL, K-P., and SIEMON, B. 1998. Examples of 1D inversion of multifrequency HEM data from 3-D resistivity distribution. *Exploration Geophysics*, Vol. 29, 133–141.

SENGPIEL, K-P., and SIEMON, B. 2000. Advanced inversion methods for airborne electromagnetic exploration. *Geophysics*, Vol. 65, 183–192.

SINHA, A K. 1977. *Dipole electromagnetic mapping of permafrost terrains: theoretical developments and computer programs.* Geological Survey of Canada, Paper 77-13.

SMITH, T., HOVERSTEN, M., GASPERIKOVA, E., and MORRISON, F. 1999. Sharp boundary inversion of 2D magnetotelluric data. *Geophysical Prospecting*, Vol. 47, no. 4, 469–486.

TIKHONOV, A N., and ARSENIN, V Y. 1977. *Solution of ill-posed problems.* (Washington D.C.: Winston.)

WISEN, R., AUKEN, E., and DHALIN, T. 2005. Combination of 1D laterally constrained inversion and 2D smooth inversion of resistivity data with a priori data from boreholes. *Near-Surface Geophysics*, Vol. 3, no. 2, 71-78.

ZHANG, Z. 2003. 3D resistivity mapping of airborne EM data. *Geophysics*, Vol. 68, no. 6, 1896–1905.

ZHDANOV, M S. 2002. *Geophysical inverse theory and regularisation problems.* (Amsterdam: Elsevier.)

ZHDANOV, M S., and TARTARAS, E. 2002. Three-dimensional inversion of multitransmitter electromagnetic data based on the localized quasi-linear approximation. *Geophysical Journal International*, Vol. 148, no. 3, 506–519.